



ELSEVIER

Available online at www.sciencedirect.com

SCIENCE @ DIRECT®

Journal of
Electroanalytical
Chemistry

Journal of Electroanalytical Chemistry 554–555 (2003) 61–69

www.elsevier.com/locate/jelechem

An electrochemical time-of-flight technique with galvanostatic generation and potentiometric sensing

Katarzyna Slowinska^a, Stephen W. Feldberg^b, Marcin Majda^{a,*}

^a Department of Chemistry, University of California, Berkeley, CA 94720-1460, USA

^b Building 815, Brookhaven National Laboratory, Upton, NY 11973-5000, USA

Received 30 September 2002; received in revised form 16 December 2002; accepted 6 January 2003

Abstract

A variation of an electrochemical time-of-flight (ETOF) technique is described and illustrated with the test cases involving electrochemically generated Ag^+ and H^+ ions in aqueous solutions of different viscosity and ionic strength. Similar to the earlier ETOF methods, the new ETOF technique also relies on photolithographically fabricated microelectrode devices. It uses a constant current (rather than potentiostatic) mode of generation of redox species and, unlike earlier approaches, it uses potentiometric (rather than amperometric) monitoring of the rates of their diffusion to the sensor microelectrode. The unknown D -values can be obtained by direct comparison between the experimentally obtained and digitally simulated E vs t transients. Digital simulations were based on simple hemi-cylindrical diffusion between the microband generator modeled as a hemi-cylinder and sensor microband electrode assumed to be infinitesimally small. This model approximates well the experimental results as long as the spacing between the two microband electrodes is approximately equal to or greater than twice their width. Discrepancies between theory and experiment may also arise due to the double-layer charging of the sensor | solution interface, and migration effects.

© 2003 Elsevier Science B.V. All rights reserved.

Keywords: Band microelectrode; Hemi-cylindrical diffusion

1. Introduction

Electrochemical time-of-flight (ETOF) is a methodology involving dual-electrode, generation–collection-type experiments in which rates of diffusion of redox species produced at a generator electrode are monitored at a collector electrode as a function of time. These techniques are designed to measure diffusion constants of redox species as well as diffusive electron transport in media of interest. While early ring-disk-type experiments [1] reflect, in principle, the general features of a generator–collector technique, the ETOF methods typically involve lithographically fabricated microband electrodes or interdigitated arrays of microelectrodes. The first such ETOF experiment described by Feldman et al. [2] was developed to measure rates of electron hopping in redox polymer films. The ETOF techniques were further developed by Wrighton and coworkers [3–

6], and used to measure rates of diffusion of ions in polymeric and fluid solution media. Theoretical modeling was done by Bard et al. [7] and Fosset et al. [8]. In two most recent reports, Williams and coworkers [9] described a dual microband titration method with a galvanostatically driven generator and an amperometric collector. In the other, Wittek et al. [10] adopted the ETOF methodology to the measurements of transport in Langmuir monolayer films at the air | water interface. The 2D ETOF was used to measure the rate of electron hopping in solid films of $\text{Os}(\text{DPP})_3(\text{ClO}_4)_2$ (DPP, 4,7-diphenyl-1,10-phenanthroline) and to investigate lateral diffusion of redox-active amphiphiles on the water surface [10].

The common feature of the various ETOF methods is a constant potential electrogeneration of redox species and a time-resolved, amperometric monitoring of their arrival at the collector microelectrode. Specifically, such experiments are initiated by an application of a potential step or a short potential pulse to a generator microelectrode, and synchronized recording collector current vs

* Corresponding author. Fax: +1-510-642-0269.

E-mail address: majda@socrates.berkeley.edu (M. Majda).

time transients at constant potential. In all cases, diffusion constants (D) are obtained by measuring arbitrarily defined transit times (τ) and relating their values to those obtained in the calibration experiments run with species of known D -values [9]. Since properly defined transit times are inversely proportional to the diffusion coefficient, the calibration experiments allow one to construct linear working curves reflecting the following general relationship of the amperometric ETOF methods:

$$\tau = \frac{Kd^2}{D} \quad (1)$$

Here d is the distance between the generator and collector electrodes, and the constant K depends on the geometry of a generator–collector device, on the mode of the experiment (pulse or step), and on the specific definition of transit time. Thus, once a working curve is obtained, amperometric ETOF serves as a reliable method of measuring diffusion constants of redox species in media of interest with the advantage of not requiring knowledge of the concentration of the diffusing species [10].

Considering the generality of ETOF, one realizes that hydrogen ions may constitute an exception. While generation of the hydrogen ions as well as their reduction can be easily accomplished electrochemically, a constant potential operation of a collector microelectrode required in the amperometric ETOF cannot be implemented in this case due to the hydrogen ion involvement in the water autoprotolysis equilibrium. Indeed, we found experimentally that it is essentially impossible to select a potential of a collector microelectrode that it is both sufficiently negative to yield a diffusion-controlled current due to reduction of protons diffusing from the generator electrode, and not too negative to prevent reduction of the hydrogen ions present in aqueous solutions due to water autoprotolysis. The background hydrogen ion reduction inevitably increases the pH near the collector electrode and thus introduces a positive error in measurements of proton transit times [11].

To overcome these difficulties, we began to consider alternative strategies in ETOF measurements. The one that we present in this report involves an open-circuit potentiometric measurement at the collector electrode instead of the usual constant potential amperometric mode. It also relies on a controlled rate (galvanostatic) formation of redox species at the generator. Indeed, the results presented below show that the new strategy is successful in the measurements of hydrogen ion diffusion constant. However, our main goal in developing the new mode of ETOF stems from our long-term interest in understanding proton mobilities in complex, structurally heterogeneous biological systems. We anticipate

that such future investigations will be likely to involve systems of substantially smaller dimensions (e.g. thin-layer-type cells) and thus of substantially higher resistance. In such cases, accurate control of the electrode potential required in the amperometric ETOF is difficult due to IR losses. The galvanostatic mode of generating redox species, and potentiometric monitoring of the rates of their arrival at the sensor presently implemented in the new ETOF will be intrinsically advantageous.

Below, we present a detailed account of the development of this new mode of ETOF. We demonstrate its capabilities using a simple case of Ag^+ ion generation and sensing in aqueous media of different viscosities. Finally, initial results concerned with the proton ETOF with galvanostatic generation and potentiometric sensing are also presented.

While in this report we are concerned solely with “open solution”-type experiments in which diffusion evolves hemi-cylindrically around microelectrodes, we consider these studies to be an essential prelude to our further investigations of interfacial proton transport.

2. Experimental

2.1. Reagents

House-distilled water was passed through a three-cartridge Millipore purification train consisting of a Macropure pretreatment, an organic-free cartridge for removal of trace organic contaminants, an ion exchanger, and a 0.2 μm hollow-fiber final filter for removing particles. The resistivity of the resulting water (DI water) was $\approx 18.3 \text{ M}\Omega \text{ cm}$. A silver cyanide-plating solution was purchased from Transene Co. and used as directed. Potassium tetrachloropalladate (99.99%, Alfa Aesar), iridium(IV) chloride (99.95%, Alfa Aesar), oxalic acid dihydrate (99%, Aldrich), hydrogen peroxide (30%, EM Science), lithium perchlorate (99.99%, Aldrich), sodium nitrate (ACS certified, Fischer Scientific), sulfuric acid (reagent grade, EM Science), sucrose (99+%, Aldrich), and 3-mercaptopropyltrimethoxysilane (MPS; 95%, Aldrich) were all used as received.

2.2. Fabrication and characterization of the generator–sensor microband devices

The design of these devices (see Fig. 1) features two parallel 10- μm wide microband electrodes separated by a gap of different widths, w , of 4, 20, 40, 60, and 80 μm . Each of the two 2-mm long microbands can be independently addressed via $4 \times 6 \text{ mm}^2$ contact pads. Glass slides (Corning 2947) used as substrates were first cleaned in a hot chromic acid solution for ~ 30 min, repeatedly rinsed with DI water, and dried under nitrogen. Next, they were treated with MPS to provide

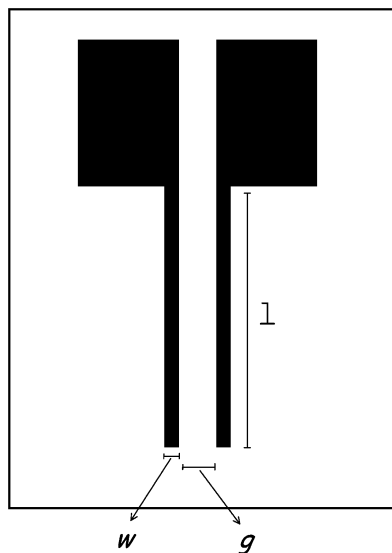


Fig. 1. A schematic drawing of the generator–sensor device. The width (w) and the length (l) of the microband electrodes are $10\ \mu\text{m}$ and $2\ \text{mm}$, respectively. The interelectrode gap (g) is $4, 20, 40, 60,$ or $80\ \mu\text{m}$.

adequate adhesion for the subsequent vapor-deposited gold layer. The detailed MPS treatment procedure was described in our recent report [10]. Vapor deposition of 80-nm thick gold films followed at $\sim 5 \times 10^{-7}$ Torr. The gold-coated glass slides were then used to fabricate the devices described above using a standard, photolithographic procedure with a wet etching. The mask and the devices were produced in the UCB Microfabrication Laboratory. At this point, the devices were modified to adopt them to a particular ETOF-type experiment. In the case of the silver ETOF experiments, both generator and sensor microband electrodes were electroplated with silver using a commercial silver-plating solution and protocol. This involved ca. $1\ \text{min}$ of galvanostatic electrolysis with $5\ \text{mA cm}^{-2}$ current density and resulted in $\sim 0.7\text{-}\mu\text{m}$ thick silver films. Those were measured with a stylus profilometer (Alfa-step 100; Tencor, Inc.). Much thinner Ag films (ca. $10\ \text{nm}$) were formed on the sensor microelectrodes. Modification of the devices used in the proton ETOF experiments involved a constant potential ($+0.25\ \text{V vs SCE}$) deposition of Pd (100 atomic layers) on the generator microelectrode from a $1.0\ \text{mM}$ solution of potassium tetrachloropalladate in $0.1\ \text{M}$ sulfuric acid [12]. Immediately prior to the ETOF experiments, the generator was loaded with hydrogen from an aqueous, $\text{pH } 6.5$ electrolyte in a 10-s constant potential electrolysis at $-1.1\ \text{V vs SCE}$. The sensor microband electrodes of the ETOF devices were prepared by an electrochemically induced precipitation of iridium(IV) oxide [13,14]. The process was initiated by a constant current density ($1\ \text{mA cm}^{-2}$) electroreduction of an oxalate ligand of an iridium oxalate complex. The IrO_2

films thus obtained were $20\text{--}120\ \text{nm}$ in thickness depending on the time of the electroreduction. These sensor electrodes were calibrated by measuring their open-circuit potential during a series of standard additions of sulfuric acid to a calibration solution. Following these modifications, the width of every generator electrode was measured microscopically (Reichert microscope) with a precision of $0.2\ \mu\text{m}$, as this is one of the input parameters in the digital simulations. All electrochemical and ETOF experiments were carried out at $22 \pm 0.5\ ^\circ\text{C}$.

2.3. Measurements of the Ag^+ and H^+ diffusion constants

The diffusion coefficient of Ag^+ (in $0.1\ \text{M LiClO}_4$) was determined by cyclic voltammetry ($v = 1.0\ \text{V s}^{-1}$) in a series of solutions of increasing Ag^+ concentration obtained by a standard addition method. A Pt disk microelectrode ($5\ \mu\text{m}$ radius) was polished before each measurement in order to avoid changes of the disk surface area due to silver deposition. To determine the diameter of the disk electrode, a similar set of experiments was carried out in the $0.5\ \text{M KCl}$ solutions with increasing concentrations of $\text{Ru}(\text{NH}_3)_6^{3+}$. To interpret the slope of the I vs $[\text{Ru}(\text{NH}_3)_6^{3+}]$ plot in terms of the disk radius, the value of the diffusion constant of $\text{Ru}(\text{NH}_3)_6^{3+}$ was measured voltammetrically using a controlled growth mercury electrode (CGME; BAS, Inc.) of known surface area. The latter was precisely measured by weighing a number of identical mercury drops generated by CGME. The diffusion coefficient of Ag^+ in $0.1\ \text{M LiClO}_4$ thus determined was $1.53 \pm 0.02 \times 10^{-5}\ \text{cm}^2\ \text{s}^{-1}$. The proton diffusion coefficient was measured using the same precisely calibrated microdisk electrode. To avoid surface poisoning during electroreduction of the hydrogen ions, the disk microelectrode was coated with a catalytic layer ($\sim 3\text{--}5$ monolayers) of palladium. The diffusion coefficient of H^+ in $0.10\ \text{M NaNO}_3$ was determined to be $8.4 \pm 0.4 \times 10^{-5}\ \text{cm}^2\ \text{s}^{-1}$. In view of this rather lengthy procedure used in the measurements of the diffusion constants, the Ag^+ and proton diffusion coefficients in the electrolytes of different concentrations (0.01 and $1.0\ \text{M}$) were calculated using the following relationship: $D = D^0(1 - \frac{1}{2}Ac^{1/2})$, where D^0 is the diffusion constant in the limit of infinitely dilute electrolyte solutions and $A = 0.5115$ for water at $25\ ^\circ\text{C}$ [15]. The validity of this relationship was verified by correlating the measured and calculated D -values of $\text{Ru}(\text{NH}_3)_6^{3+}$ in solutions of different electrolyte concentrations. The experimental results were found to be in agreement with the theory within ca. 2% .

2.4. Instrumentation

All electrochemical measurements were performed with a CH Instruments Model 660A electrochemical analyzer. The instrument was customized by a potentiometry adapter to measure the potential difference between the sensor and a common reference electrode in addition (during chronopotentiometric experiments) to the measurements of the potential of the working electrode. This is possible through a simultaneous two-channel recording. The maximum sampling rate of each channel of this instrument is 2.5 ms. The resolution of the potential measurements is better than 0.5 mV.

3. Results and discussion

3.1. Description of the method

A description of the dual microelectrode devices used in all the experiments is given in Section 2 (see also Fig. 1). In the experiments concerned with silver ion diffusion, both the generator and sensor microelectrodes were plated with silver. The ETOF experiments were carried out in the $\text{AgNO}_3 + \text{LiClO}_4$ solutions of specific concentrations given below. A typical experiment was initiated by applying a constant current step (I_{gen}) to the generator electrode. This triggered the measurements of the potential of the sensor microelectrode as a function of time. Fig. 2 shows a cross-sectional view of a generator–sensor device with the concentration profiles of the electrogenerated Ag^+ ions that diffuse away from the generator microband. As we discuss this below, we determined that in most cases transport of the electrochemically generated ions can be described quantitatively by hemi-cylindrical diffusion. The diffusion constants of the Ag^+ ions in aqueous media of variable viscosity (adjusted with sucrose) were measured voltammetrically with a Pt microdisk electrode as described in Section 2. These values were then used as input

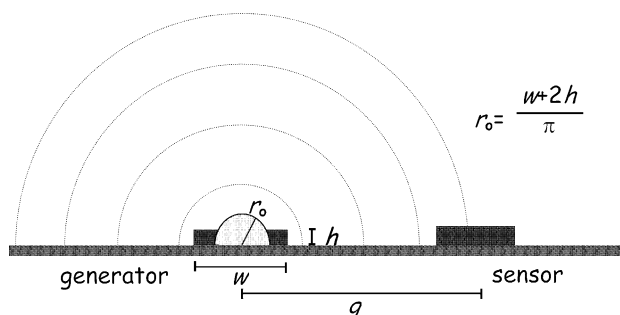


Fig. 2. Schematic cross-sectional view of the generator–sensor device illustrating the hemi-cylindrical diffusion of species away from the generator microband. The inset equation is the expression used to calculate the effective radius of the cylinder using the physical dimensions of the generator microband electrode.

parameters in the digital simulations of the E vs t transients.

Computer simulations were executed using implicit finite difference simulation with hemi-cylindrical geometry [16]. The radius, r_0 , of the hemi-cylindrical electrode modeling the microband generator was chosen so that the area of the hemi-cylinder equaled the area of an experimental generator of the same length (see Fig. 2):

$$r_0 = \frac{w + 2h}{\pi} \quad (2)$$

We assumed that the sensing electrode is infinitesimally small and located at a specified distance, r , from the center of the generating electrode. Thus, the pertinent value of r equals to the interelectrode gap, g , measured as the center-to-center distance between two microband electrodes as shown in Fig. 2. For a specified generating flux, the concentration of the generated species was reported to change in the reversible potential of the sensing electrode as a function of time. For example, the change in the potential of the Ag sensor electrode was expressed as

$$E - E_{\text{init}} = E_{\text{Ag}}^0 + \frac{RT}{F} \ln \left[\frac{\Delta[\text{Ag}^+] + [\text{Ag}^+]_{\text{in}}}{[\text{Ag}^+]_{\text{in}}} \right] \quad (3)$$

where $\Delta[\text{Ag}^+]$ is the electrogenerated change in the concentration of Ag^+ and $[\text{Ag}^+]_{\text{in}}$ is the initial bulk concentration of Ag^+ . Similarly, Eq. (3) can be rewritten to express the change in the potential of the H^+ -sensor electrode. We will assume that $[\text{H}^+]_{\text{in}} > 10^{-6}$ M and that no buffering ions are present. We established that both the silver and the iridium dioxide pH-sensor microelectrodes exhibit Nernstian responses with slopes of 60 ± 1 and 80 ± 2 mV per decade, respectively. The super-Nernstian slope of the iridium oxide sensor has been noted in the literature [14,17]. Knowing these experimentally determined slope values, the effective temperature, T , was calculated and used as an input parameter (Eq. (3)) in the simulations.

The hemi-cylindrical generator electrode and a small sensor are reasonable approximations of the experimental setup when the interelectrode gap is sufficiently large (i.e. 10- μm wide bands separated by ≥ 20 μm). We also point out that the agreement between the experimental data and this simple hemi-cylindrical diffusion model is expected only when the sensor microelectrode can be assumed not to perturb the local concentration of the diffusing species. Since sensors operate at open circuit, this means that the charge required to change the potential of the sensor electrode is small and does not affect the concentration of the diffusing ions in the vicinity of the sensor. A more detailed discussion of these limitations is given below.

A comparison of the experimental and simulated E vs t transients for a set of experiments involving micro-electrode devices with different interelectrode gaps is shown in Fig. 3. Similarly, Fig. 4 features a comparison of the transients obtained in media of different viscosities. The agreement between the experiments and theory indicates that hemi-cylindrical diffusion offers a good description of the diffusion processes in spite of the fact that the widths of the generator and sensor microband electrodes (w_g and w_s) are relatively large, and thus depart from the model assumptions in which w_g is represented by the equivalent radius, r_0 , and $w_s = 0$. The use of hemi-cylindrical diffusion as the basis of the digital simulations becomes less effective when devices with gaps substantially smaller than $20\ \mu\text{m}$ are used. In these cases, an increasing contribution of a linear diffusion component is expected to result in faster rising E vs t transients. While we did not systematically investigate the magnitude of such a deviation as a function of g , the transients in Fig. 5 recorded with a $g = 4\ \mu\text{m}$ device do show the breakdown of the hemi-cylindrical diffusion theory. We note that the positive deviation in the E vs t transients in Fig. 5 could not be caused by migration because the experiments were done in the solutions of high supporting electrolyte concentration, and because decreasing current density does not diminish the extent of the deviation between the experiment and simulation. A more detailed discussion of the migration effects is given below.

Data in Figs. 3 and 4 also show that, unlike the amperometric ETOF method, this technique does not require calibration. E vs t transients obtained experimentally with a device of known dimensions for a

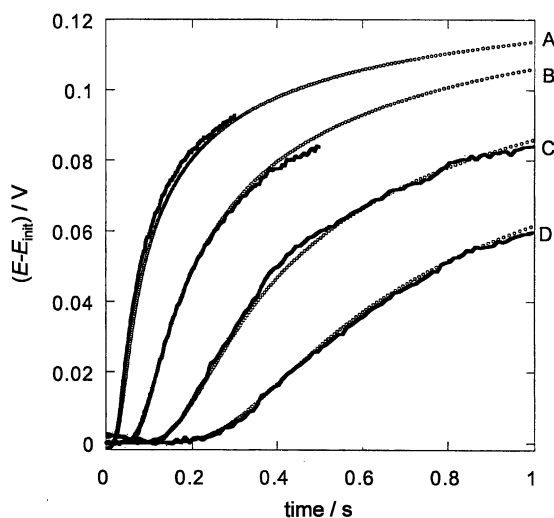


Fig. 3. A set of the experimental (line) and simulated (open circles) E vs t transients of a sensor microelectrode obtained with devices of different gap widths: (A) $20\ \mu\text{m}$, (B) $40\ \mu\text{m}$, (C) $60\ \mu\text{m}$, and (D) $80\ \mu\text{m}$. The experiments were carried out in $0.6\ \text{mM}\ \text{AgNO}_3 + 0.1\ \text{M}\ \text{LiClO}_4$ solution. The generator current was $0.1\ \text{mA}$. The simulations were generated with a Ag^+ diffusion coefficient of $1.53 \times 10^{-5}\ \text{cm}^2\ \text{s}^{-1}$.

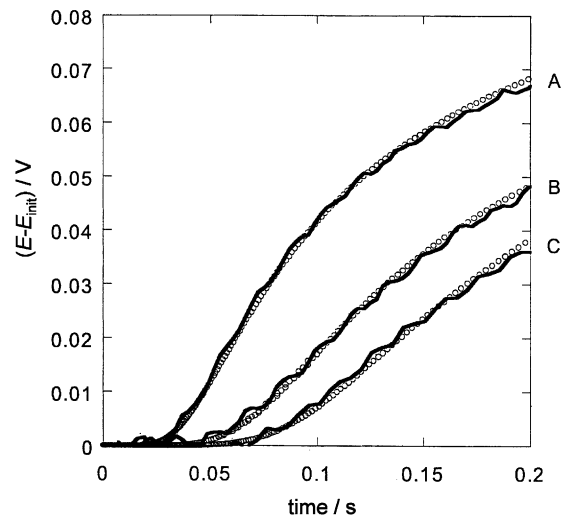


Fig. 4. A set of the experimental (line) and simulated (open circles) sensor E vs t transients obtained with a $20\text{-}\mu\text{m}$ gap device in $0.6\ \text{mM}\ \text{AgNO}_3 + 1\ \text{M}\ \text{LiClO}_4$ solution containing 0% (A), 20% (B), and 28% (C) ($w\ \text{v}^{-1}$) sucrose. The generator current was $0.05\ \text{mA}$. The simulations were generated with Ag^+ diffusion coefficients of $1.24 \times 10^{-5}\ \text{cm}^2\ \text{s}^{-1}$ (A), $0.64 \times 10^{-5}\ \text{cm}^2\ \text{s}^{-1}$ (B), and $0.44 \times 10^{-5}\ \text{cm}^2\ \text{s}^{-1}$ (C).

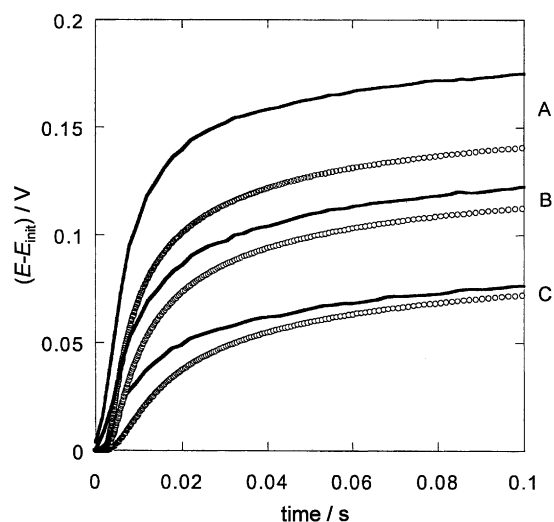


Fig. 5. A set of the experimental (line) and simulated (open circles) sensor E vs t transients for a $4\text{-}\mu\text{m}$ gap device recorded in $0.6\ \text{mM}\ \text{AgNO}_3 + 1\ \text{M}\ \text{LiClO}_4$ solution at the generator currents of $0.15\ \text{mA}$ (A), $0.05\ \text{mA}$ (B), and $0.01\ \text{mA}$ (C). The simulations were generated with Ag^+ diffusion coefficient of $1.24 \times 10^{-5}\ \text{cm}^2\ \text{s}^{-1}$.

species of an unknown D can be compared directly with digital simulations run for different D -values to match the experimental result.

3.2. Double-layer charging and migration effects

Agreement between the digitally simulated and experimental E vs t transients of the type presented in Figs. 3 and 4 can be expected only when the latter are recorded in a certain range of the experimentally

controlled parameters. Specifically, we observed that a significant delay in the rising portion of the sensor's potential transient may be observed whenever the rate of a potential change is large and when flux of the electrogenerated species in the vicinity of the sensor microband is small.

To understand the phenomena underlying this general observation, consider again the schematic representation of the hemi-cylindrical diffusion governing the transport of the electrogenerated species between generator and sensor in Fig. 2. First, it is important to note that only a small fraction of the electrochemically generated Ag^+ ions diffuses in the direction of the sensor microband. Next, one must appreciate the fact that the increase of the sensor's potential in response to an increasing concentration of the silver ions requires reduction of some Ag^+ ions at the sensor to charge its surface to a new value reflecting that increase. In the present case, the sensor microelectrode is at open circuit. Yet, any increase of its potential (dE) in response to the increase of the Ag^+ concentration involves double-layer charging. It is accomplished by the reduction of silver ions to increase the positive charge (dQ) on the sensor's surface in proportion to its differential capacitance ($C_{\text{dl}}(E)$) and its surface area (A), $dQ = C_{\text{dl}}A dE$. In view of Faraday's law, the differential quantity of the silver ions required to be reduced, dN (mol), can be expressed by

$$dN = \frac{C_{\text{dl}}(E)A dE}{nF} \quad (4)$$

As mentioned above, the resulting decrease of the silver ion concentration near the sensor's surface due to this double-layer charging should be small or else a delay in the E vs t transients is observed. In other words, delays due to the double-layer charging should be expected whenever the rate of increase of the sensor potential is high and the flux of Ag^+ ions diffusing from the generator electrode is small. This situation is not unlike a balance between supply and demand. Supply refers here to an instantaneous flux of the silver ions at the sensor's surface. Its magnitude depends on I_{gen} and inversely on the interelectrode gap. Demand in this case is constant. It refers to a constant number of moles of silver ions, dN , that must be reduced to increase the potential of a sensor of a given surface area by a fixed value. (This assumes a constant value of C_{dl} , see Eq. (4).) However, it is important to note that, in view of the Nernstian equation, dN is independent of the initial (background) Ag^+ concentration ($[\text{Ag}^+]_{\text{in}}$). Thus, when $[\text{Ag}^+]_{\text{in}}$ is low, even a small flux of silver ions may require a large change of the sensor potential. This is when "demand" is non-negligible relative to "supply" and a delay in the sensor's response is to be expected.

Overall, a combination of three variables determines the magnitude of the time delay due to the double-layer charging. These are $[\text{Ag}^+]_{\text{in}}$, I_{gen} , and g . The effect of each of these parameters on the shape of the E vs t transients is shown in Figs. 6–8. In these figures, the values of the other two of the three parameters were chosen so that a range of double-layer charging delays from large to zero could be illustrated. It is characteristic in all these cases that the delays affect only the rising portion of the E vs t transients, and that even in the cases of severely delayed transients (e.g. see transients A and B in Fig. 6) their plateau values agree well with the theoretical expectations. Data in Figs. 6–8 clearly suggest that the double-layer charging delays are easier to minimize if the background Ag^+ concentration is not too low. As the $[\text{Ag}^+]_{\text{in}}$ is increased, the double-layer charging delays are easier to avoid but the overall magnitude of the potential change decreases (see Fig. 6). Another way to minimize the double-layer charging delay that can be deduced from Eq. (1) is to use microband devices with very small sensor electrodes. Our devices with $w_s = 10 \mu\text{m}$ were not optimized in this respect. (Using the same microfabrication methodology, the width of the sensor microband electrodes could be decreased by as much as an order of magnitude.) Eq. (1) also suggests that electrode surface modification that would decrease its interfacial capacitance could also be advantageous. However, delays due to slow electron transfer kinetics might offset the low capacitance advantage of a chemically modified surface. Finally, we note that an additional delay could result from double-layer charging of the generator microelectrode.

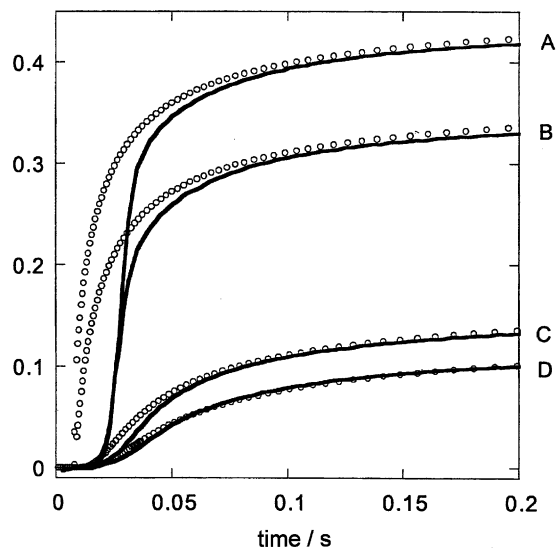


Fig. 6. A set of the experimental (line) and simulated (open circles) sensor E vs t transients obtained with a 20- μm gap device in 0.1 M LiClO_4 solutions in which the concentrations of Ag^+ ions were 10^{-8} M (A), 10^{-7} M (B), 10^{-4} M (C), and 7×10^{-4} M (D). The generator current was 0.2 mA. The simulations were generated with Ag^+ diffusion coefficient of $1.53 \times 10^{-5} \text{ cm}^2 \text{ s}^{-1}$.

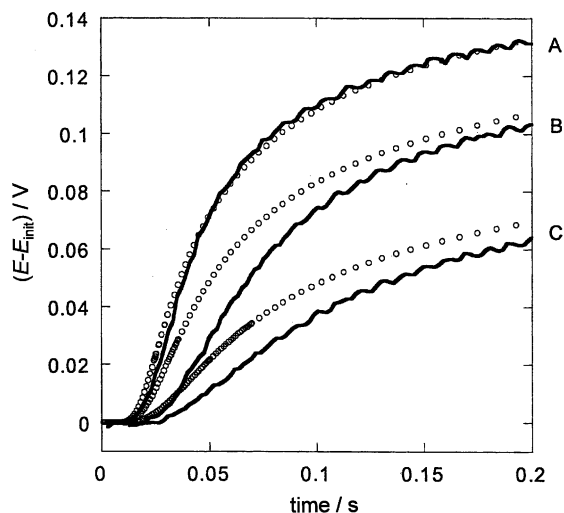


Fig. 7. A set of the experimental (line) and simulated (open circles) sensor E vs t transients obtained with a 20- μm gap device in a 0.3 mM AgNO_3 +0.1 M LiClO_4 solution at the generator currents of 0.2 mA (A), 0.08 mA (B), and 0.04 mA (C). The simulations were generated with Ag^+ diffusion coefficient of $1.53 \times 10^{-5} \text{ cm}^2 \text{ s}^{-1}$.

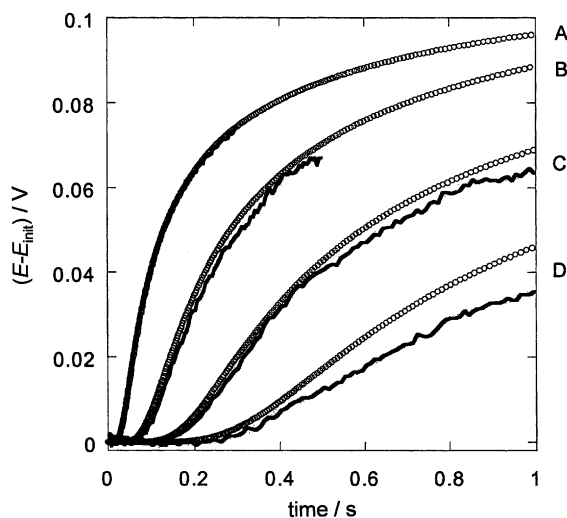


Fig. 8. A set of the experimental (line) and simulated (open circles) sensor E vs t transients recorded with the generator–sensor devices of different gap widths in 0.6 mM AgNO_3 +0.1 M LiClO_4 solution. The generator current was 0.05 mA. Curves A–D correspond to gap widths of 20, 40, 60, and 80 μm , respectively. The simulations were generated with Ag^+ diffusion coefficient of $1.53 \times 10^{-5} \text{ cm}^2 \text{ s}^{-1}$.

In the galvanostatic mode, the time delay due to generator electrode double-layer charging is inversely proportional to the selected current magnitude and proportional to the electrode size and its interfacial capacitance. Even in the case of the smallest generator current of 0.01 mA used in these measurements, the double-layer charging time delay is less than 1 ms and thus is insignificantly small.

Since an increased generator current helps minimize the double-layer charging (see Fig. 7), one should be

concerned as to whether migration could accelerate Ag^+ transport. Indeed, under such conditions, when the concentration of the supporting electrolyte is insufficiently high, a faster increase of the sensor potential can be observed relative to the purely diffusive transients predicted by a digital simulation. This is shown in Fig. 9.

3.3. Electrochemical proton time-of-flight

One can envision several strategies for electrochemically generating hydrogen ions. The results presented below were obtained in the experiments involving electrooxidation of hydrogen from a Pd(H) microband electrode. The exact protocol of these experiments is given in Section 2. Briefly, the gold generator microband electrode of the ETOF devices was first overcoated with ca. 100 atomic layers of palladium using a literature procedure [12]. Hydrogen was introduced by electroreduction of water. A typical loading level of hydrogen in Pd was 60 at.%. This was measured coulometrically by a complete electrooxidation of hydrogen. Pd(H) microelectrodes thus prepared could sustain galvanostatic oxidation of hydrogen at $I_{\text{gen}} = 2 \mu\text{A}$ (a maximum value used in the proton ETOF experiments below) for ca. 30 s. The sensor microband electrode was coated with a thin film of IrO_2 (ca. 20 nm in thickness) by an electrochemically induced precipitation using a Ir^{IV} oxalate solution [13,14]. These microelectrochemical sensors exhibited linear plots of E vs pH over a pH range 2.0–11.0 with a super-Nernstian slope of $78 \pm 1 \text{ mV}$ per decade. In order to demonstrate the performance of these devices in the electrochemical proton

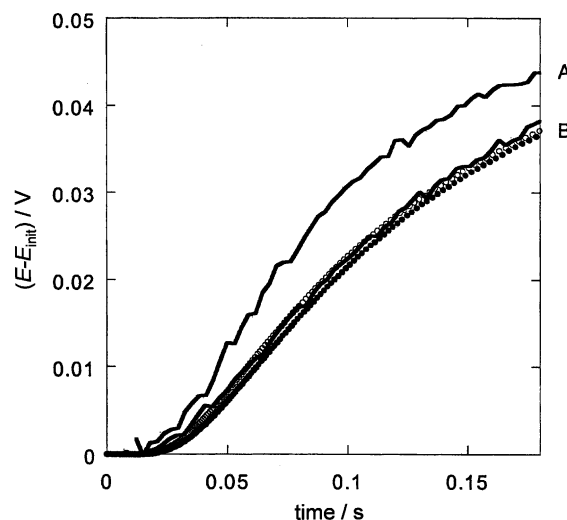


Fig. 9. A set of the experimental (line) and simulated (open circles) sensor E vs t transients obtained with a 20- μm gap device in 0.6 mM AgNO_3 solutions also containing 0.01 M LiClO_4 (A) and 1.0 M LiClO_4 (B). The generator current was 0.01 mA. The simulations were generated with Ag^+ diffusion coefficients of $1.62 \times 10^{-5} \text{ cm}^2 \text{ s}^{-1}$ (A) and $1.24 \times 10^{-5} \text{ cm}^2 \text{ s}^{-1}$ (B).

time-of-flight experiments, we recorded E vs t transients for several different generator currents. In addition, to induce some changes in the proton diffusion constant, several ETOF experiments were carried out in electrolyte solutions of different concentrations. It is well known that the diffusion coefficients of ions depend on the ionic strength of electrolytes according to the following equation [15]:

$$D = D^0(1 - \frac{1}{2}Ac^{1/2}) \quad (5)$$

where D^0 is the diffusion constant in the limit of infinitely dilute electrolyte solutions and $A = 0.5115$ for water at 25 °C. The results of these proton ETOF experiments together with the corresponding simulated transients are shown in Fig. 10. The comparison is satisfactory. Small discrepancies between the experimental and simulated transients could be due to the characteristics of the IrO₂ sensing layers. These are subjects of ongoing investigations.

4. Conclusions

ETOF with galvanostatic generation and potentiometric sensing introduced in this report is similar to the previously developed amperometric ETOF method. However, the modifications implemented in this version of ETOF resulted in several tangible advantages. First, the new method relies on a direct comparison (fit) of the recorded E vs t transients with simple digital simulations based on hemi-cylindrical diffusion approximation. In most previously reported cases, a working curve

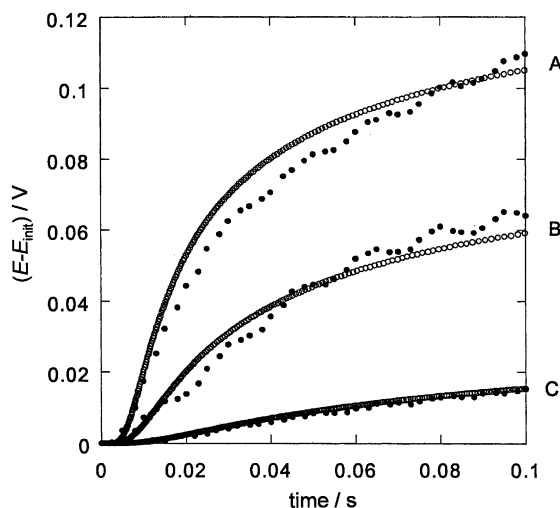


Fig. 10. A set of the experimental (closed circles) and simulated (open circles) sensor E vs t transients recorded with a 20- μ m gap device in 0.05 mM HNO₃+0.1 M NaNO₃ solutions (A, B) and in 0.05 mM HNO₃+1 M NaNO₃ solution (C). The generator currents were 2.0 μ A (A), 1.0 μ A (B), and 0.70 μ A (C). The simulations were generated with H⁺ diffusion coefficients of 8.4×10^{-5} cm² s⁻¹ (A, B) and 6.9×10^{-5} cm² s⁻¹ (C).

approach (τ vs $1/D$, see Eq. (1)) requiring a set of calibration experiments was used in the amperometric ETOF [3–6,9]. Second, we believe that our version of ETOF is more compatible with the measurements requiring resistive media, and in the investigations of systems where thin-layer-cell-type configuration results in high IR losses relative to the amperometric ETOF. The galvanostatic mode of generating redox species and potentiometric monitoring of the rates of their arrival at the sensor are intrinsically advantageous relative to the controlled potential mode. In the latter case, accurate control of the electrode potential is burdened with an uncertainty of IR loss. In listing this as a potential advantage, we project future applications of the ETOF technique as not only a method to determine diffusion constants but, perhaps more importantly, as a method to characterize complex media by studying diffusive transport of species with known D -values. Finally, the possibility of measuring rates of proton diffusion is a singular advantage deriving from the potentiometric mode of sensing in our ETOF method. As discussed above, proton involvement in the autoprotolysis equilibria did not allow us to rely on the amperometric ETOF in these experiments.

These advantages come with some limitations. The double-layer charging delays of the sensor electrode can be severe and must be dealt with judiciously, as shown in the previous sections. Migration is another phenomenon that could introduce a discrepancy which ultimately would yield an error in the determination of D -values. One potential source of error in the time evolution of the sensor's potential transients which we did not discuss is the sluggish kinetics (electron transfer or ion adsorption–desorption) at the sensor|electrolyte interface. While these processes were apparently sufficiently rapid in the two cases we have investigated thus far not to introduce any distortions in the sensor response, interfacial kinetics could introduce errors in other cases and should be carefully evaluated. We point out that the rapid mass transports that can be reached with the generator–collector devices featuring narrow interelectrode gaps offer an opportunity to investigate response rates of potentiometric sensors systematically. The rise time of the IrO₂ pH sensor is currently a subject of our ongoing investigations.

Acknowledgements

We acknowledge the donors of the Petroleum Research Fund, administered by the ACS, for partial support of this research. Additional support was provided at UCB by the National Science Foundation (CHE-0079225).

References

- [1] W.J. Albery, M. Hitchman, Ring-disc Electrodes, Clarendon Press, Oxford, 1971.
- [2] B.J. Feldman, S.W. Feldberg, R.W. Murray, J. Phys. Chem. 91 (1987) 6558.
- [3] S. Licht, V. Cammarata, M.S. Wrighton, Science 243 (1989) 1176.
- [4] V. Cammarata, D.R. Talham, R.M. Crooks, M.S. Wrighton, J. Phys. Chem. 94 (1990) 2680.
- [5] S. Licht, V. Cammarata, M.S. Wrighton, J. Phys. Chem. 94 (1990) 6133.
- [6] H.B. Tatistcheff, I. Fritsch-Faules, M.S. Wrighton, J. Phys. Chem. 97 (1993) 2732.
- [7] A.J. Bard, J.A. Crayston, G.P. Kittlesen, T.V. Shea, M.S. Wrighton, Anal. Chem. 58 (1986) 2321.
- [8] B. Fosset, C. Amatore, J. Bartlet, R.M. Wightman, Anal. Chem. 63 (1991) 1403.
- [9] H. Rajantie, J. Strutwolf, D.E. Williams, J. Electroanal. Chem. 500 (2001) 108.
- [10] M. Wittek, G. Möller, M.J. Johnson, M. Majda, Anal. Chem. 73 (2001) 870.
- [11] K. Slowinska, M. Majda, unpublished results.
- [12] M. Baldauf, D.M. Kolb, Electrochim. Acta 38 (1993) 2145.
- [13] K. Yamanaka, Jpn. J. Appl. Phys. 28 (1989) 632.
- [14] S.A.M. Marzouk, S. Ufer, R.P. Buck, T.A. Johnson, L.A. Dunlap, W.E. Cascio, Anal. Chem. 70 (1998) 5054.
- [15] J.O'M. Bockris, A.K.N. Reddy, Modern Electrochemistry: An Introduction to an Interdisciplinary Area, vol. 1, Plenum Press, New York, 1970, pp. 382–385 (Chapter 4.4.10).
- [16] D. Britz, Digital Simulation in Electrochemistry, 2nd revised and extended ed., Springer, Berlin, 1988.
- [17] S. Yao, M.J. Madou, Electrochem. Soc. 148 (2001) H29.